

Quasicrystalline order and a crystal-liquid state in a soft-core fluid

A.J. Archer*, A.M. Rucklidge† and E. Knobloch#

**Department of Mathematical Sciences, Loughborough University, Loughborough LE11 3TU, UK*

†*Department of Applied Mathematics, University of Leeds, Leeds LS2 9JT, UK*

#*Department of Physics, University of California at Berkeley, Berkeley, CA 94720, USA*

A two-dimensional system of soft particles interacting via a two-length-scale potential is studied. Density functional theory and Brownian dynamics simulations reveal a fluid phase and two crystalline phases with different lattice spacing. Of these the larger lattice spacing phase can form an exotic periodic state with a fraction of highly mobile particles: a crystal liquid. Near the transition between this phase and the smaller lattice spacing phase, quasicrystalline structures may be created by a competition between linear instability at one scale and nonlinear selection of the other.

PACS numbers: 61.50.Ah, 61.44.Br, 05.20.-y, 64.70.D-

Crystals are ordered arrangements of atoms or molecules with rotation and translation symmetries. Quasicrystals (QCs), discovered in 1982 [1], lack the lattice symmetries of crystals and yet have discrete Fourier spectra. QCs have been found not only in metals but also in colloidal systems [2, 3], mesoporous silica [4] and soft-matter systems [5]. The latter can form micelles [6, 7], e.g., from dendrimers or block copolymers, comprising a hydrophobic polymer core surrounded by a corona of flexible hydrophilic polymer chains. Theoretical approaches to investigating the stability of metallic or micellar QCs often involve minimising an appropriate energy, but the principle underlying their stability is not known [8, 9].

Patterns with quasicrystalline structure, or quasipatterns, were discovered in Faraday wave experiments in the 1990s; two mechanisms for stabilizing these were identified [10]. The first, relevant to experiments in Ref. [11], involves one length scale and may lead to a stable quasipattern [12]. The second, involving coupling between an unstable scale and weakly damped (or weakly excited) waves with a different length scale, is relevant to the experiments in Refs. [13–16], and was explored in [17–22]. This mechanism can also operate for soft-matter QCs [23–26]. Here, we observe a dynamic mechanism for forming QCs involving two length scales that is qualitatively different: the system first forms a small length scale crystal. Only when this phase is almost fully formed (i.e., the dynamics is far into the nonlinear regime) does the longer length scale start to appear, leading to the formation of QCs. This process occurs in a region of the phase diagram where the linear growth of density fluctuations in a quenched uniform fluid selects the shorter scale but nonlinear stability favors a longer scale.

The effective coarse-grained interaction potentials between the centres of mass of polymers, dendrimers or other such macromolecules, are soft. By this we mean that they are finite for all separation distances r , because the centre of mass of such soft objects does not necessarily coincide with any individual monomer. The soft effective pair potential between such particles can be approximated as $V(r) = \epsilon e^{-(r/R)^n}$. Simple linear poly-

mers in solution correspond to the case $n = 2$ with the length R of order the radius of gyration and the energy ϵ for a pair of polymers to fully overlap of order $2k_B T$, where k_B is Boltzmann's constant and T is the temperature [27–33]. Dendrimers, due to the nature of their chemical architecture, can have an effective interaction with a higher value of n ; such systems form so-called cluster crystals [33] and there has been much interest in soft potential models for these systems [34–40].

Here we consider a model two-dimensional system of soft particles that interact via the potential

$$V(r) = \epsilon e^{-(r/R)^8} + \epsilon A e^{-(r/R_s)^8}. \quad (1)$$

This potential is finite for all r and has a shoulder when the parameter $A \neq 0$, with two length scales. The radius of the core is R and the radius of the shoulder is $R_s > R$; the energy for complete overlap is $(1 + A)\epsilon$. Such a potential is a simple coarse-grained model for the effective interaction between dendrimers, star polymers or micelles formed, e.g., from block copolymers, which have a stiff hydrophobic core surrounded by a corona of flexible hydrophilic chains. A related, but piecewise constant potential is used in Ref. [25]. The limits (i) $A \rightarrow 0$ or (ii) $A \rightarrow \infty$ and $\epsilon \rightarrow 0$ with $\epsilon A = \text{constant}$ both result in systems with a single crystal phase. In the following we set the dimensionless interaction energy parameter $\beta\epsilon = 1$, where $\beta = (k_B T)^{-1}$, and fix the ratio of the two length scales to be $R_s/R = 1.855$ (see below).

We use density functional theory (DFT) [41–43] to study this system. The grand free energy is

$$\begin{aligned} \Omega[\rho(\mathbf{r})] = & k_B T \int d\mathbf{r} \rho(\mathbf{r}) [\ln \Lambda^2 \rho(\mathbf{r}) - 1] \\ & + \mathcal{F}_{ex}[\rho(\mathbf{r})] + \int d\mathbf{r} (\Phi(\mathbf{r}) - \mu) \rho(\mathbf{r}), \quad (2) \end{aligned}$$

which is a functional of the one-body (number) density of the particles, $\rho(\mathbf{r})$, where $\mathbf{r} = (x, y)$. The first term is the ideal-gas contribution to the free energy \mathcal{F}_{id} , Λ is the thermal de Broglie wavelength, μ is the chemical potential, $\Phi(\mathbf{r})$ is any external potential that may be confining the system, and $\mathcal{F}_{ex}[\rho(\mathbf{r})]$ is the excess Helmholtz

free energy from the interactions between the particles. The equilibrium density profile is that which minimizes $\Omega[\rho(\mathbf{r})]$; the corresponding minimum is the thermodynamic grand potential of the system. For a system in the bulk fluid state (i.e., where $\Phi(\mathbf{r}) \equiv 0$), the minimizing density is uniform, $\rho = \rho_0$. However, for other state points, when the system freezes to form a solid, Ω is minimized by a nonuniform $\rho(\mathbf{r})$, exhibiting sharp peaks. For the systems of soft-core particles considered here, one may approximate \mathcal{F}_{ex} as [27]:

$$\mathcal{F}_{ex}[\rho(\mathbf{r})] = \frac{1}{2} \int d\mathbf{r} \int d\mathbf{r}' \rho(\mathbf{r}) V(|\mathbf{r} - \mathbf{r}'|) \rho(\mathbf{r}'). \quad (3)$$

This functional generates the random phase approximation (RPA) for the pair direct correlation function $c^{(2)}(\mathbf{r}, \mathbf{r}') \equiv -\beta \frac{\delta^2 \mathcal{F}_{ex}}{\delta \rho(\mathbf{r}) \delta \rho(\mathbf{r}')} = -\beta V(|\mathbf{r} - \mathbf{r}'|)$ [41–43]. If we assume that these are Brownian particles with dynamics

$$\dot{\mathbf{r}}_i = -\Gamma \nabla_i U(\{\mathbf{r}_i\}, t) + \Gamma \mathbf{X}_i(t), \quad (4)$$

where the index $i = 1, \dots, N$ labels particles, $U(\{\mathbf{r}_i\}, t) = \sum_{i=1}^N \Phi(\mathbf{r}_i) + \sum_{i \neq j} V(\mathbf{r}_i - \mathbf{r}_j)$ is the potential energy of the system and $\mathbf{X}_i(t)$ is a white noise term, we can investigate the dynamics of the system using Dynamic Density Functional Theory (DDFT) [44–47] in the form

$$\frac{\partial \rho(\mathbf{r}, t)}{\partial t} = \Gamma \nabla \cdot \left[\rho(\mathbf{r}, t) \nabla \frac{\delta \Omega[\rho(\mathbf{r}, t)]}{\delta \rho(\mathbf{r}, t)} \right], \quad (5)$$

where $\rho(\mathbf{r}, t)$ is now the time-dependent nonequilibrium one-body density profile and $\Gamma \equiv \beta D$ is the mobility. Here D is the diffusion coefficient. In deriving Eq. (5) we have used the equilibrium free energy $\mathcal{F} = \mathcal{F}_{id} + \mathcal{F}_{ex}$ to approximate the unknown nonequilibrium free energy.

Fig. 1(a) shows the equilibrium phase diagram calculated using Picard iteration [48] of the DFT Euler–Lagrange equation, starting either from the profile for a nearby state point or a uniform density profile with a small random value added to each point. As the fluid density is increased, the system freezes to form one of two distinct solid phases (Fig. 2): for larger values of A the system forms crystal A, a hexagonal crystal with a large lattice spacing, but for smaller values of A it forms crystal B, a hexagonal crystal with a much smaller lattice spacing. The red regions in Fig. 1(a) denote thermodynamic coexistence between two different phases at the same temperature, pressure and chemical potential.

To understand the phase diagram we study the structure and stability of a uniform liquid with density ρ_0 and $\Phi(\mathbf{r}) \equiv 0$. We follow [41, 46, 49, 50] and expand Eq. (5) in powers of $\tilde{\rho}(\mathbf{r}, t) \equiv \rho(\mathbf{r}, t) - \rho_0$. Retaining only linear terms, we find that the growth/decay of different Fourier modes of wave number k follows $\hat{\rho}(k, t) = \hat{\rho}(k, 0) \exp[\omega(k)t]$, where $\omega(k)$ satisfies the dispersion relation [46, 50]

$$\omega(k) = -\Gamma k_B T k^2 (1 - \rho_0 \hat{c}(k)). \quad (6)$$

Here $\hat{c}(k)$ is the Fourier transform of the pair direct correlation function; within RPA $\hat{c}(k) = -\beta \hat{V}(k)$, where $\hat{V}(k)$ is the Fourier transform of the pair potential in Eq. (1). In an equilibrium fluid the static structure factor $S(k) \equiv [1 - \rho_0 \hat{c}(k)]^{-1} > 0$ for all k ; such a fluid is therefore stable [51]. Within RPA the two length scales in the pair potential lead, for certain ranges of parameter values, to a static structure factor $S(k)$ with two peaks. Fig. 1(b)–(d) shows that as A increases the smaller k peak in $S(k)$ grows and comes to dominate the larger k peak. Fig. 1(e)–(g) shows analogous behavior of $\omega(k)$ at several points in or on the boundary of the linearly unstable region $\omega(k_{max}) = 0$, where k_{max} is the wave number of the *higher* peak (blue dashed line in Fig. 1(a)): as A increases the instability shifts from large k (Fig. 1(g)) to small k (Fig. 1(e)). The short and long length scales are simultaneously marginally stable at $A = 1.067$ and $\rho_0 R^2 = 2.95$ (Fig. 1(f)); this point lies on the pink dotted line in Fig. 1(a) corresponding to a pair of equal height peaks in $\omega(k)$. Above (below) this line, the peak at smaller (larger) wave number k is higher, indicating that the longer (shorter) length scale density fluctuations grow the fastest. The black double dotted lines indicate the location of $\omega(k_{max}) = 0$ for the *lower* peak in $\omega(k)$. When the system is quenched from a stable liquid state to a state point with density ρ_0 above the blue dashed line, certain wave numbers will grow as described by $\omega(k)$.

Fig. 2(c), shows the density profile of the larger lattice spacing crystal A phase for a state point not far from the transition to the smaller lattice spacing crystal B phase. However, the panel below displaying $\ln[R^2 \rho(\mathbf{r})]$ reveals an interconnected network of channels between the density peaks. The particles contributing to this part of the density profile are fluid in the sense that they can move freely throughout the whole system, unlike the majority of the particles that are located in density peaks at multiply occupied lattice sites. This is the crystal-liquid (CL) state. This state minimizes the free energy for $A > A_{co}$, where A_{co} is the value at coexistence. Interfaces between the different phases in Fig. 2 are present whenever these coexist (cf. [52, 53]), but these will be discussed elsewhere.

To confirm the existence of the CL state we calculate the density profile for a system within a square confining potential Φ of size $L \times L$ with hard walls, and compare the results with Brownian dynamics (BD) simulations, i.e., simulations of N particles evolving according to Eq. (4). Averaging over the positions of the particles to calculate the density profile, we find remarkably good agreement between the DFT and the BD results (Fig. 3). The resulting system thus consists of two dynamically distinct populations, in contrast to related systems [54–57] in which the dynamics of all the particles are identical. In Fig. 4 we display, for $\beta\mu = 39$, the percentage of mobile particles in crystal A as a function of A , obtained by integration over all portions of the density profile that

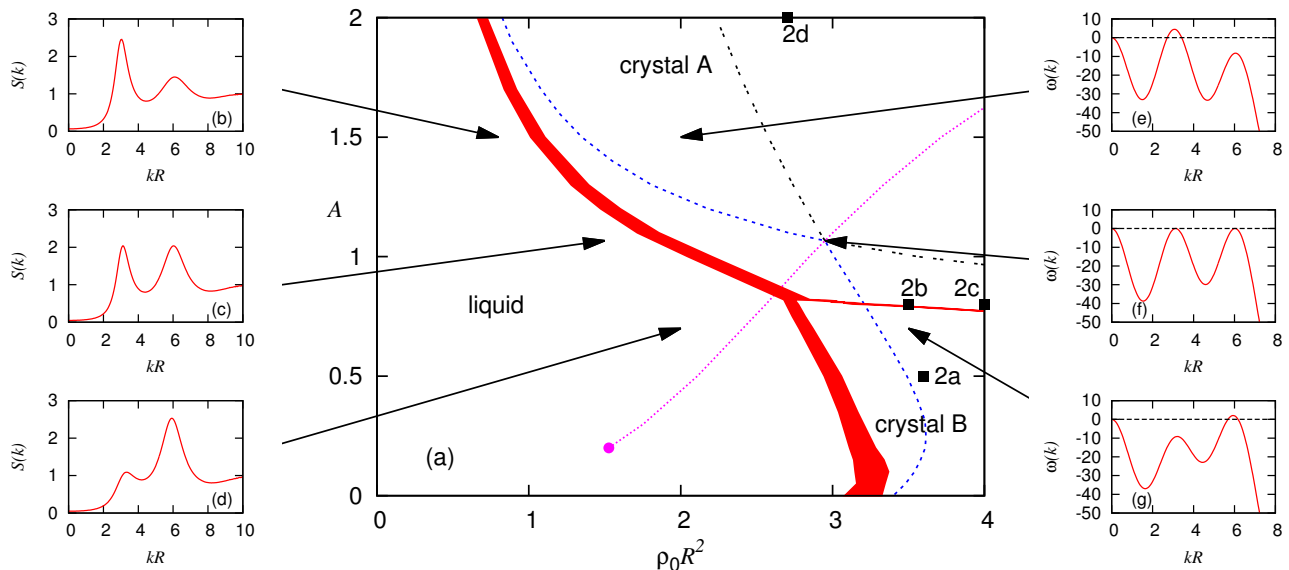


FIG. 1: (color online) Phase diagram, static structure factor $S(k)$ and dispersion relation $\omega(k)$ for $\beta\epsilon = 1$ and $R_s/R = 1.855$. (a) The bulk system phase diagram in the $(\rho_0 R^2, A)$ plane. The system exhibits a uniform fluid phase and two crystal phases: the larger lattice spacing crystal A phase and the smaller lattice spacing crystal B phase. The regions filled in red denote areas where there is two-phase coexistence between the different phases. The blue dashed line denotes the linear instability threshold for the liquid phase while the pink dotted line terminating in a circle is the locus where the two peaks in the dispersion relation (6) have the same height. The circle denotes the point where the smaller k peak disappears. (b)–(d) $S(k)$ for (b) $(\rho_0 R^2, A) = (0.8, 1.5)$, (c) $(1.5, 1.067)$, (d) $(2, 0.7)$. (e)–(g) $\omega(k)$ for (e) $(\rho_0 R^2, A) = (2, 1.5)$, (f) $(2.95, 1.067)$, (g) $(3.5, 0.7)$. The state points corresponding to the profiles in Fig. 2 are marked with the symbol ■.

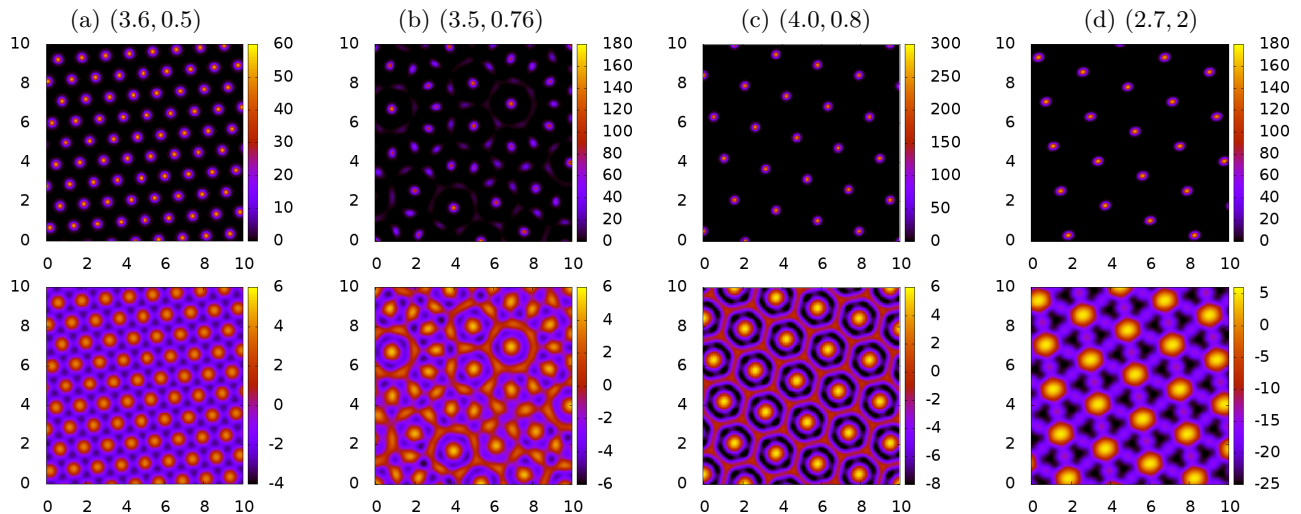


FIG. 2: (color online) Density profiles from DFT showing $R^2\rho(\mathbf{r})$ (upper panels) and $\ln[R^2\rho(\mathbf{r})]$ (lower panels). Profiles for: (a) $(\rho_0 R^2, A) = (3.6, 0.5)$ (typical of the small length scale crystal B), (b) $(3.5, 0.76)$, (c) $(4.0, 0.8)$ (both near the transition from crystal A to crystal B) and (d) $(2.7, 2)$ (typical of the large length scale crystal A). These state points are marked ■ in Fig. 1(a). The profiles in (b) show quasicrystalline ordering with numerous defects, while (c) reveals a network of connected density, indicating that the particles in this part of the crystal are fluid, and able to move throughout the system. There are also similar connected fragments in the disordered (b) profile, but because of the disorder, these do not percolate the system.

are a distance $0.65R$ away from the centre of the density peaks. Particles contributing to this portion of the density are defined to be mobile. For $\beta\mu = 0.39$, the two crystal phases coexist at $A_{\text{co}} \approx 0.75$; the proportion of mobile particles increases rapidly as $A \rightarrow A_{\text{co}}^+$ and reaches

over 7% at this value of the chemical potential. In fact, as A is further decreased it is this growing number that triggers the formation of the smaller length scale crystal: these mobile particles freeze to form the extra peaks of crystal B.

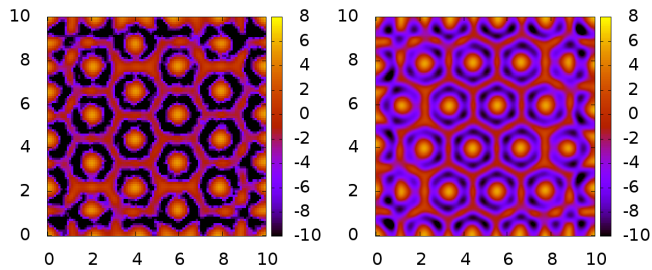


FIG. 3: $\ln[R^2\rho(\mathbf{r})]$ for a system of $N = 600$ particles with $(\rho_0 R^2, A) = (4.0, 0.8)$ confined in a square region of side $L = 10R$ obtained from BD simulations (left panel) and DFT (right panel). The system forms crystal A with a density profile consisting of an array of peaks surrounded by a connected network within which the particles are free to move – the CL state.

Observation of metastable QCs: A striking aspect of the phase diagram in Fig. 1(a) is that the phase transition between the two different crystal phases (thin red region) is well away from where the two peaks in the dispersion relation have the same height (pink dotted line). A uniform system quenched to the region above the coexistence of the two crystal phases but below this line will initially generate small length scale density fluctuations and the system behaves as if it were going to form crystal B. However, the true minimum of the free energy is the larger length scale crystal. Thus, as growing density fluctuations reach the nonlinear regime, the system seeks to go to the longer length scale structure but the smaller length scale imprinted from the linear growth regime leads to frustration. Sometimes the system is able to evolve to the larger length scale crystal; at other times it stays stuck in the metastable small length scale crystal B structure. However, often the system forms a state with density peaks on both length scales, but no long range order. In Fig. 5 we display two rather striking density profiles calculated near state point 2b in Fig. 1(a). The upper profile was calculated using Picard iteration starting from random initial conditions. The density profile has many defects, but it has definite quasicrystalline ordering, as can be seen from the corresponding Fourier transform. The lower panels in Fig. 5 show a defect-free QC approximant, started from carefully chosen initial conditions. The two wavenumbers $k_1 R = 3.2$ and $k_2 R = 6.0$ corresponding to the maxima in $\omega(k)$ are indicated in the Fourier transforms.

The Picard iteration of the Euler–Lagrange equation corresponds to fictitious dynamics since it does not conserve the total number of particles in the system, $N \equiv \int d\mathbf{r}\rho(\mathbf{r})$. The true dynamics is governed by the DDFT Eq. (5). Evolving this equation is much slower, but in most cases the same qualitative behavior is observed. The supplementary material below shows time-dependent QC formation obtained using DDFT. The conserved DDFT dynamics does however lead to a

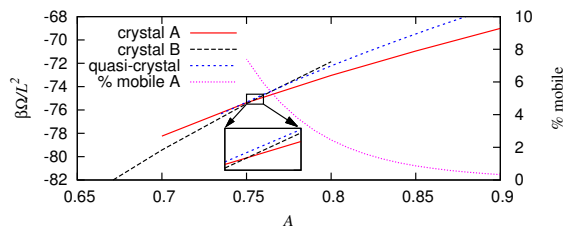


FIG. 4: Grand potential density for $\beta\mu = 39$ as a function of A for the two different crystal structures and the QC solution displayed in Fig. 5. There is a point where all three have almost the same free energy, but the QC solution is never the global minimum of the free energy (see inset). The crystal A phase is of CL type throughout the range of A shown. We also display the % of mobile particles in the crystal A phase.

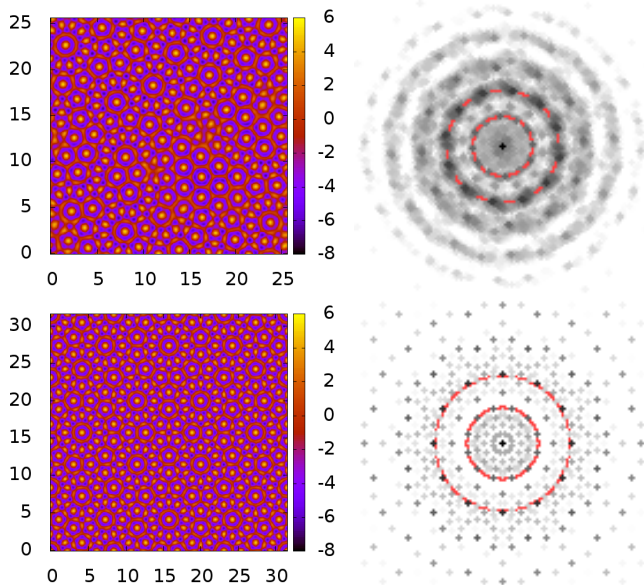


FIG. 5: Left: $\ln[R^2\rho(\mathbf{r})]$ from DFT, for $(\rho_0 R^2, A) = (3.5, 0.8)$. Right: the corresponding Fourier transforms. The 12-fold symmetry is indicative of QC ordering. The upper profile was obtained from random initial conditions, while the lower one was started from initial conditions with QC symmetry.

higher likelihood of getting stuck in the crystal B structure formed in the initial linear growth regime. For $\beta\epsilon = 1$, $R_s/R = 1.855$ the QCs we find are never the minimum free energy state (Fig. 4). The QC state in Fig. 5 remains stable against small perturbations for $1.77 < R_s/R < 2.18$, but we have not calculated the full phase diagram for $R_s/R \neq 1.855$ (at $R_s/R = 1.885$ the two marginally stable wave numbers (Fig. 1(f)) are very close to the ratio $2\cos(\pi/12) = 1.93$, favoring 12-fold QCs). We believe it may be possible to use nonlinear dynamics techniques [22] to compute the stability properties of these states by reducing the DDFT description in Eq. (5) to a phase field crystal model, cf. [50, 58–61]. We expect that the observed QC formation mechanism

(linear growth of one length scale, but nonlinear selection favoring another) may well apply more generally.

Acknowledgement: This work was supported in part by the National Science Foundation under grant DMS-1211953 (EK). We are grateful for discussions with R. Lifshitz and P. Olmsted.

-
- [1] D. Shechtman, I. Blech, D. Gratias, and J. W. Cahn, *Phys. Rev. Lett.* **53**, 1951 (1984).
- [2] A. R. Denton and H. Löwen, *Phys. Rev. Lett.* **81**, 469 (1998).
- [3] D. V. Talapin, E. V. Shevchenko, M. I. Bodnarchuk, X. C. Ye, J. Chen, and C. B. Murray, *Nature* **461**, 964 (2009).
- [4] C. H. Xiao, N. Fujita, K. Miyasaka, Y. Sakamoto, and O. Terasaki, *Nature* **487**, 349 (2012).
- [5] T. Dotera, *Isr. J. Chem.* **51**, 1197 (2011).
- [6] X. B. Zeng, G. Ungar, Y. S. Liu, V. Percec, S. E. Dulcey, and J. K. Hobbs, *Nature* **428**, 157 (2004).
- [7] S. Fischer, A. Exner, K. Zielske, J. Perlich, S. Deloudi, W. Steurer, P. Lindner, and S. Forster, *Proc. Nat. Acad. Sci. USA* **108**, 1810 (2011).
- [8] A. S. Keys and S. C. Glotzer, *Phys. Rev. Lett.* **99**, 235503 (2007).
- [9] C. L. Henley, M. de Boissieu, and W. Steurer, *Philosophical Magazine* **86**, 1131 (2006).
- [10] H. W. Müller, *Phys. Rev. E* **49**, 1273 (1994).
- [11] B. Christiansen, P. Alstrom, and M. T. Levinsen, *Phys. Rev. Lett.* **68**, 2157 (1992).
- [12] B. A. Malomed, A. A. Nepomnyashchiĭ, and M. I. Tribelskiĭ, *Sov. Phys. JETP* **69**, 388 (1989).
- [13] W. S. Edwards and S. Fauve, *Phys. Rev. E* **47**, R788 (1993).
- [14] A. Kudrolli, B. Pier, and J. P. Gollub, *Physica D* **123**, 99 (1998).
- [15] H. Arbell and J. Fineberg, *Phys. Rev. E* **65**, 036224 (2002).
- [16] Y. Ding and P. Umbanhowar, *Phys. Rev. E* **73**, 046305 (2006).
- [17] W. B. Zhang and J. Viñals, *J. Fluid Mech.* **336**, 301 (1997).
- [18] R. Lifshitz and D. M. Petrich, *Phys. Rev. Lett.* **79**, 1261 (1997).
- [19] C. M. Topaz, J. Porter, and M. Silber, *Phys. Rev. E* **70**, 066206 (2004).
- [20] A. C. Skeldon and G. Guidoboni, *SIAM J. Appl. Math.* **67**, 1064 (2007).
- [21] A. M. Rucklidge and M. Silber, *SIAM J. Appl. Dynam. Syst.* **8**, 298 (2009).
- [22] A. M. Rucklidge, M. Silber, and A. C. Skeldon, *Phys. Rev. Lett.* **108**, 074504 (2012).
- [23] R. Lifshitz and H. Diamant, *Philos. Mag.* **87**, 3021 (2007).
- [24] M. Engel and H. R. Trebin, *Phys. Rev. Lett.* **98**, 225505 (2007).
- [25] K. Barkan, H. Diamant, and R. Lifshitz, *Phys. Rev. B* **83**, 172201 (2011).
- [26] J. Rottler, M. Greenwood, and B. Ziebarth, *J. Phys.: Condens. Matter* **24**, 135002 (2012).
- [27] C. N. Likos, *Phys. Reports* **348**, 267 (2001).
- [28] J. Dautenhahn and C. K. Hall, *Macromolecules* **27**, 5399 (1994).
- [29] C. N. Likos, H. Löwen, M. Watzlawek, B. Abbas, O. Jucknischke, J. Allgaier, and D. Richter, *Phys. Rev. Lett.* **80**, 4450 (1998).
- [30] P. G. Bolhuis, A. A. Louis, J.-P. Hansen, and E. J. Meijer, *J. Chem. Phys.* **114**, 4296 (2001).
- [31] C. N. Likos and H. M. Harreis, *Condens. Matter Phys.* **5**, 173 (2002).
- [32] C. N. Likos, *Soft Matter* **2**, 478 (2006).
- [33] D. A. Lenz, R. Blaak, C. N. Likos, and B. M. Mladek, *Phys. Rev. Lett.* **109**, 228301 (2012).
- [34] A. Lang, C. N. Likos, M. Watzlawek, and H. Löwen, *J. Phys.: Condens. Matter* **12**, 5087 (2000).
- [35] A. J. Archer, C. N. Likos, and R. Evans, *J. Phys.: Condens. Matter* **16**, L297 (2004).
- [36] B. M. Mladek, D. Gottwald, G. Kahl, M. Neumann, and C. N. Likos, *J. Phys. Chem. B* **111**, 12799 (2007).
- [37] A. J. Moreno and C. N. Likos, *Phys. Rev. Lett.* **99**, 107801 (2007).
- [38] C. N. Likos, B. M. Mladek, D. Gottwald, and G. Kahl, *J. Chem. Phys.* **126**, 224502 (2007).
- [39] S. van Teeffelen, A. J. Moreno, and C. N. Likos, *Soft Matter* **5**, 1024 (2009).
- [40] A. Nikoubashman, G. Kahl, and C. N. Likos, *Soft Matter* **8**, 4121 (2012).
- [41] R. Evans, *Adv. Phys.* **28**, 143 (1979).
- [42] R. Evans, *Fundamentals of Inhomogeneous Fluids* (Dekker, New York, 1992).
- [43] J. F. Lutsko, *Adv. Chem. Phys.* **144**, 1 (2010).
- [44] U. Marini, B. Marconi, and P. Tarazona, *J. Chem. Phys.* **110**, 8032 (1999).
- [45] U. Marini, B. Marconi, and P. Tarazona, *J. Phys.: Condens. Matter* **12**, A413 (2000).
- [46] A. J. Archer and R. Evans, *J. Chem. Phys.* **121**, 4246 (2004).
- [47] A. J. Archer and M. Rauscher, *J. Phys. A: Math. Gen.* **37**, 9325 (2004).
- [48] R. Roth, *J. Phys.: Condens. Matter* **22**, 063102 (2010).
- [49] R. Evans and M. T. D. Gama, *Molec. Phys.* **38**, 687 (1979).
- [50] A. J. Archer, M. J. Robbins, U. Thiele, and E. Knobloch, *Phys. Rev. E* **86**, 031603 (2012).
- [51] J.-P. Hansen and I. R. McDonald, *Theory of Simple Liquids* (Academic, London, 1986), 2nd ed.
- [52] M. Oettel, *J. Phys.: Cond. Matt.* **24**, 464124 (2012).
- [53] B. A. Malomed, A. A. Nepomnyashchy, and M. I. Tribelsky, *Phys. Rev. A* **42**, 7244 (1990).
- [54] M. A. Glaser, G. M. Grason, R. D. Kamien, A. Kosmrlj, C. D. Santangelo, and P. Ziherl, *Europhys. Lett.* **78**, 46004 (2012).
- [55] A. Imperio and L. Reatto, *J. Phys.: Condens. Matter* **16**, S3769 (2004).
- [56] A. Imperio and L. Reatto, *J. Chem. Phys.* **124** (2006).
- [57] A. J. Archer, *Phys. Rev. E* **78**, 031402 (2008).
- [58] K. R. Elder, M. Katakowski, M. Haataja, and M. Grant, *Phys. Rev. Lett.* **88**, 245701 (2002).
- [59] Z. F. Huang, K. R. Elder, and N. Provatas, *Phys. Rev. E* **82**, 021605 (2010).
- [60] S. van Teeffelen, R. Backofen, A. Voigt, and H. Löwen, *Phys. Rev. E* **79**, 051404 (2009).
- [61] H. Emmerich, H. Löwen, R. Wittkowski, T. Gruhn, G. I. Tóth, G. Tegze, and L. Gránásy, *Adv. Phys.* **61**, 665 (2012).

SUPPLEMENTARY MATERIAL

In this supplementary material, we display examples the dynamics of quasicrystal (QC) formation, obtained (i) via Picard iteration of the DFT (Fig. 6) and (ii) from dynamical density functional theory (DDFT) (Fig. 7). In Fig. 6 we display snapshots of the logarithm of the density profile $\ln[R^2\rho(\mathbf{r})]$ as the system evolves in time, for the state point $A = 0.8$ and $\rho R^2 = 3.5$. The initial time $t = 0$ profile corresponds to a uniform density plus a small amplitude random value everywhere. The early time linear growth regime produces **one** length scale, as can be observed from Fig. 6 and also from the dispersion relation, displayed in Fig. 8. This leads to the formation of the small length-scale crystal B phase – see, e.g. the middle and right hand panels in the top row of Fig. 6. However, over time, starting from the grain boundary and regions where defects are present, the longer length scale in the system appears, leading to the formation of the QC. This occurs when the dynamics of the system is well away from the linear regime.

In Fig. 7 we display snapshots of $\ln[R^2\rho(\mathbf{r})]$ as the

system evolves in time, for the state point $A = 1.067$ and $\rho R^2 = 3.5$ (note that the linear instability line is at $\rho R^2 = 2.95$, thus this state point is quite a deep quench). The dynamics we obtain from the DDFT displayed in Fig. 7 is very similar to that obtained from the Picard iteration in Fig. 6. The DDFT dynamics is for overdamped Brownian particles, as described in our Letter (and references therein). The Picard iteration used to generate Fig. 6 does not conserve particle number. It is, however, much faster than the full DDFT and gives qualitatively similar results – compare Figs. 6 and 7. In Fig. 8 we also display the dispersion relation for the state point $A = 1.067$ and $\rho R^2 = 3.5$, which corresponds to the results in Fig. 7. Here we see that the system is linearly unstable at two distinct wavelengths. However, the peak corresponding to the smaller length scale (large k) is much higher than that of the longer length scale (small k) and so during the early time linear growth regime after the system is quenched, the smaller length scale grows much faster, so that there is no sign of the longer length scale in the early time density profile displayed in the top left hand panel of Fig. 7.

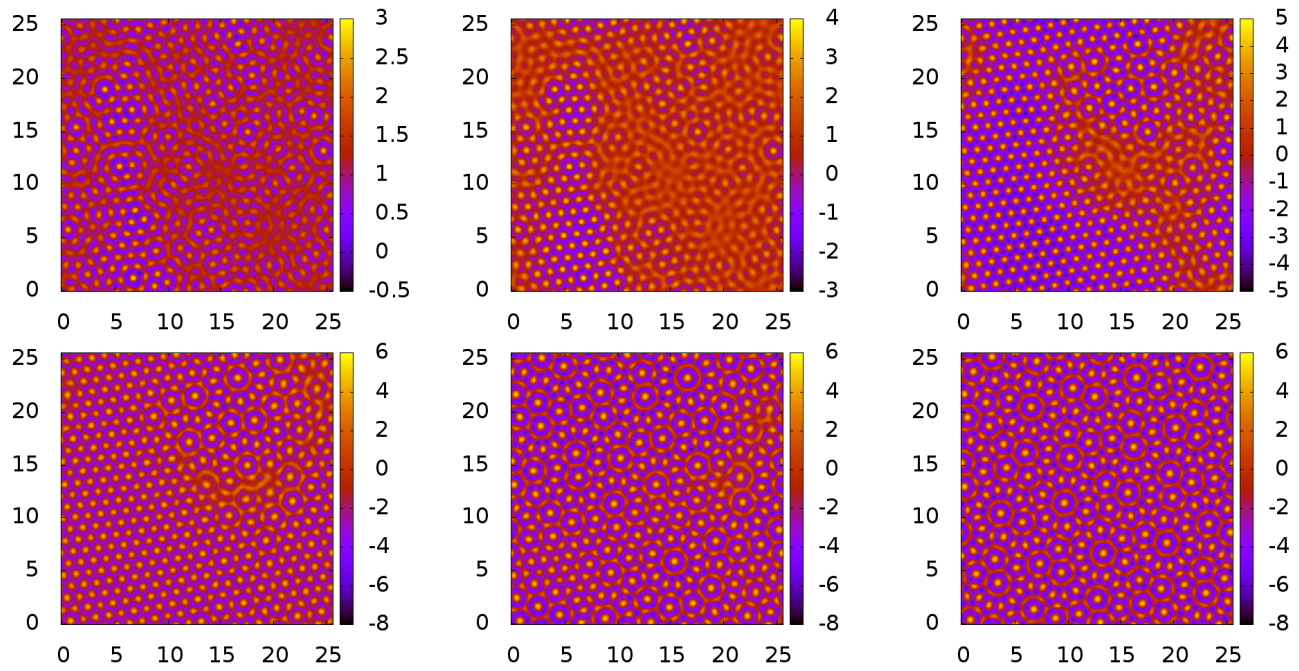


FIG. 6: Time series of profiles $\ln[R^2\rho(\mathbf{r})]$ obtained via Picard iteration, for $A = 0.8$ and $\rho R^2 = 3.5$. These show the evolution towards the equilibrium for the same state point as the results displayed in the upper panel of Fig. 4 of our Letter. The panels along the top row, from left to right, correspond to the times $t = 30, 32$ and 35 ; and along the bottom row to $t = 40, 50, 200$. Note that the system first forms (at time $t \approx 30$) the small length scale crystal. It then tries to form the longer length scale crystal. However, due to the fact that it already has the small length scale imprinted on the system, it cannot form a perfect long length scale crystal and ends up forming a disordered system with regions of QC ordering – see the final profile at time $t = 200$, or the profile in Fig. 4 of the accompanying manuscript.

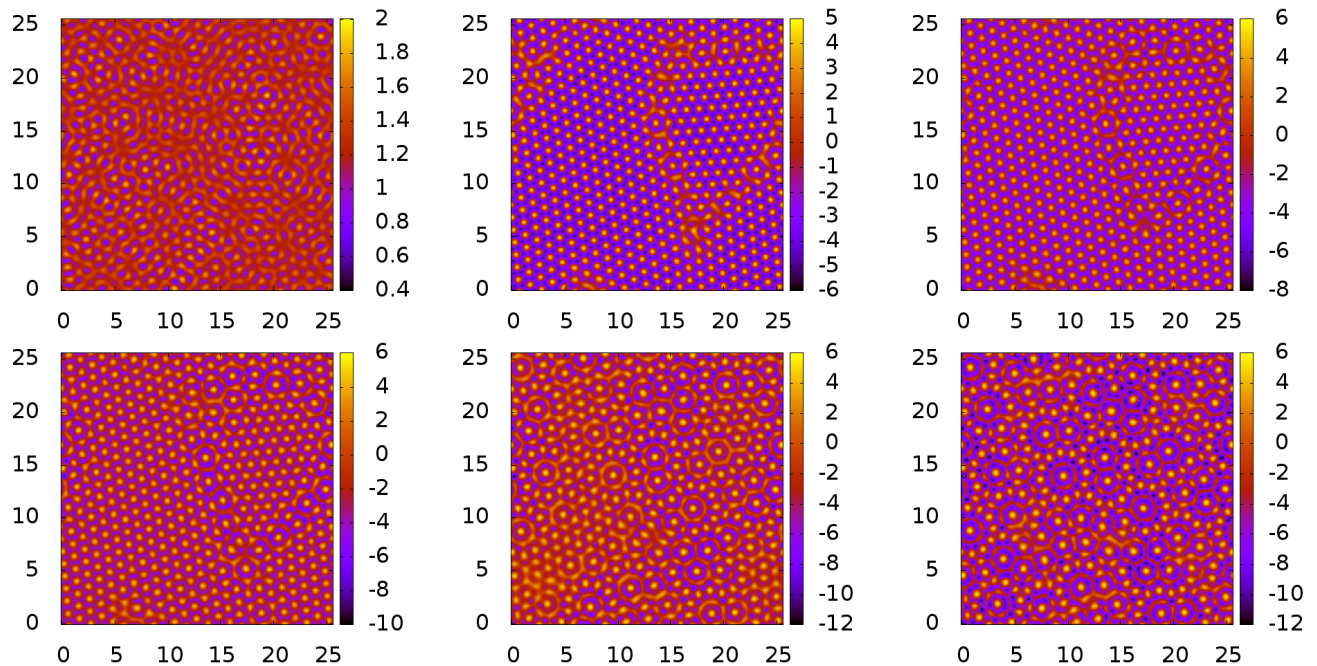


FIG. 7: Time series of profiles $\ln[R^2\rho(\mathbf{r})]$ obtained from DDFT, for $A = 1.067$ and $\rho R^2 = 3.5$. The panels along the top row, from left to right, correspond to the times $t/\tau_B = t^* = 1, 2$ and 5 ; along the bottom row the panels correspond to $t^* = 10, 20$ and 40 , where $\tau_B = \beta R^2/\Gamma$ is the Brownian timescale.

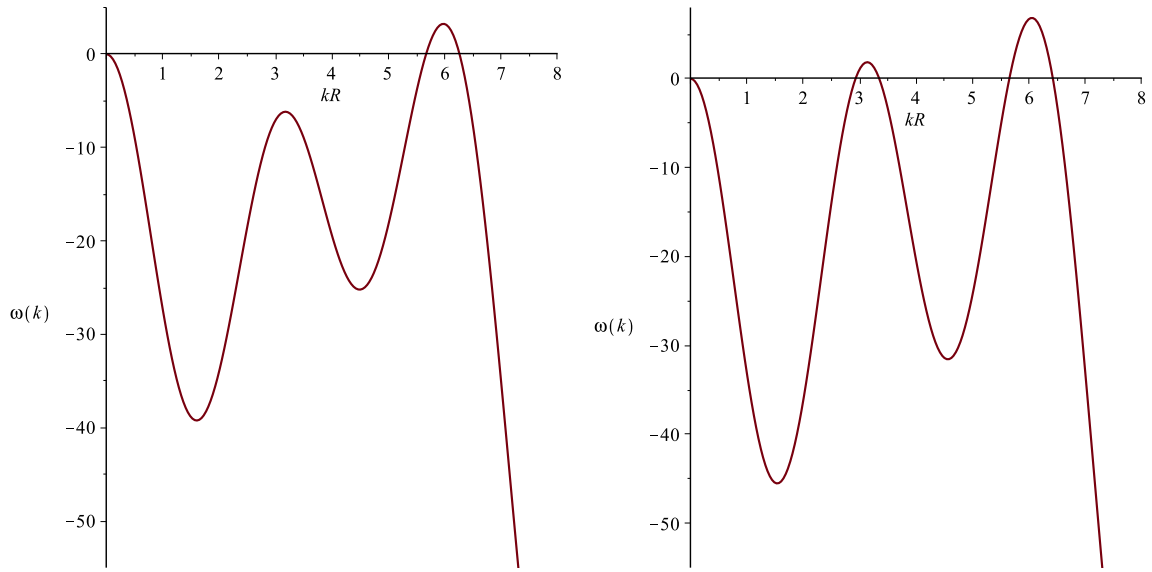


FIG. 8: The dispersion relation at the state point $A = 0.8$ and $\rho R^2 = 3.5$ (left hand plot), where the QC state displayed in Fig. 4 of our Letter is calculated. From this we see that in the linear regime, only one mode (the smaller length scale) is unstable. Density profiles from the Picard iteration to equilibrium for this state point are displayed in Fig. 6 above. Right hand plot: the dispersion relation for the state point $A = 1.067$ and $\rho R^2 = 3.5$, which corresponds to the results in Fig. 7 above.